INSTITUTE OF PHYSICS PUBLISHING JOURNAL OF PHYSICS: CONDENSED MATTER

J. Phys.: Condens. Matter **17** (2005) S3979–S3995 doi:10.1088/0953-8984/17/47/023

Molecular motors one at a time: FIONA to the rescue

Comert Kural[1], **Hamza Balci**[2] **and Paul R Selvin**[1,2,3]

[1] Center for Biophysics, University of Illinois, Urbana, IL 61801, USA
[2] Physics Department, University of Illinois, Urbana, IL 61801, USA

E-mail: selvin@uiuc.edu

Received 16 August 2005
Published 4 November 2005
Online at stacks.iop.org/JPhysCM/17/S3979

Abstract

Processive molecular motors act as intracellular transporters of a broad range of cargoes varying from organelles to messenger RNAs. Due to the nanometre range movements and complex dynamics of these motors, highly specialized tools are required to study them, in particular at the single-molecule level. Such tools are what physicists are providing for understanding these biological systems. Fluorescence based real-time localization techniques, with 1 nm spatial resolution and down to 1 ms temporal resolution (FIONA: fluorescence imaging with one-nanometre accuracy), and their applications to a group of molecular motors (myosin V, myosin VI, kinesin, and dynein) are the topics of this paper. In addition to the well established *in vitro* studies, the recent applications of these techniques to the much more challenging, but also more informative, *in vivo* realm will be discussed.

(Some figures in this article are in colour only in the electronic version)

1. FIONA

The point spread function (PSF) of an infinitely small point source has a full width at half-maximum (FWHM) of $\sim\lambda/2$ due to the diffraction limit of light [1]. This limit corresponds to a maximum resolution of about 250 nm for localizing an object using visible light ($\lambda \approx 400$–700 nm), which is far from the nanometre resolution required for studying biological phenomena at the single-molecule level. However, it has been shown that by determining the centre point of the emission pattern of an object, the position of this object can be localized very precisely [2]. Several different groups have reported that the emission pattern of fluorescent objects of different sub-wavelength sizes can be localized with approximately 1 nm accuracy when the PSF of these objects is fitted with a two-dimensional Gaussian function. These objects include single fluorophores a few nanometres in size [3], fluorescent beads several tens

[3] Address for correspondence: Loomis Laboratory of Physics, University of Illinois, 1110 W Green Street, Urbana, IL 61801, USA.

of nanometres in size [4], and membrane encapsulated organelles several hundred nanometres in size which are labelled with multiple green fluorescent proteins (GFPs) [5]. In 2003, Yildiz *et al* made the first systematic application of these findings to a molecular motor, myosin V, and showed that it is possible to track these motors with 1.5 nm accuracy and sub-second time resolution. This technique used a novel oxygen scavenging system which not only made the fluorophores brighter, i.e. they emit more photons, but also extended their lifetime, i.e. they emit photons for a longer time. In addition, total internal reflection fluorescence (TIRF) microscopy was used, which reduced the noise factors significantly below those typical for more conventional methods, e.g. epifluorescence. This new technique was colourfully named FIONA, for fluorescence imaging with one-nanometre accuracy.

The major noise factors of fluorescence imaging in which a CCD camera is used as the detector are: fluorescent background, photon noise, pixellation effects, and camera readout rate. By taking these error sources into account, the standard error of the mean (σ_μ), s.e.m., of a PSF can be calculated theoretically to be [4]

$$\sigma_{\mu_i} = \sqrt{\left(\frac{s_i^2}{N} + \frac{a^2/12}{N} + \frac{8\pi s_i^4 b^2}{a^2 N^2}\right)},$$

where s is the standard deviation of the fitted Gaussian, N is the number of collected photons, a is the pixel size, and b is the background. The first term (s_i^2/N) is the photon noise, the second term is due to the finite pixel size of the camera, and the last term is the effect of the background. As is clear from this formula, collecting more photons is the most important factor for minimizing the s.e.m. and hence maximizing the resolution.

In order to attain the best resolution, or the maximum SNR, total internal reflection fluorescence (TIRF) microscopy [6, 7] has been used in our applications. In TIRF microscopy only several hundred nanometres above the glass–water interface of the sample is illuminated and hence only fluorescence from this region contributes to the overall noise of the image, unlike in epifluorescence in which the whole depth of the sample contributes to the background noise. In a typical TIRF set-up a low noise, back-illuminated CCD camera is used to detect the fluorescence signal. Figure 1 shows an example of an emission pattern of a single fluorophore obtained through TIRF microscopy. As is clear from the image, the PSF can be fitted very well to a 2D Gaussian, and the peak position can be localized within ± 1.3 nm. As an order-of-magnitude guide, it is common to collect 10 000 photons from a single fluorophore during a 1 s integration time. Assuming a PSF FWHM of 280 nm, this many photons results in 2.8 nm, or ± 1.4 nm, resolution, i.e. the PSF divided by the square root of the number of photons. Clearly for this simple estimate to hold, it is essential that the pixellation effects should not be significant and the background noise should be much less than the net signal. Typically the SNR is around 30–35, which clearly satisfies this criterion. The pixel size varies between 86 and 160 nm for a typical FIONA set-up. The imaging is done through a magnification of 60–100$\times$ in the objective and 1.5–2.5 times in an external lens before the CCD (total magnification of 90–250 times). The current CCD cameras have a pixel size of about 16 μm, and hence a 160 magnification results in an effective pixel size of 100 nm. This pixel size in turn results in a pixellation contribution of $(a^2/12N)^{1/2} = (100)^2/12 \times 10\,000 \approx 0.3$ nm to the overall noise signal, which is about an order magnitude less than the dominant photon noise ($[s_i^2/N]^{1/2} \approx 2.8$ nm).

In the rest of the paper a brief overview of applications of FIONA to molecular motors such as myosin V, kinesin, and myosin VI will be given. Then a new technique which is based on FIONA, and is particularly useful for localizing multiple fluorophores residing within a diffraction limited spot, will be described. Finally, the recent *in vivo* experiments in which FIONA is used to track organelles within fruit fly cells will be reviewed.

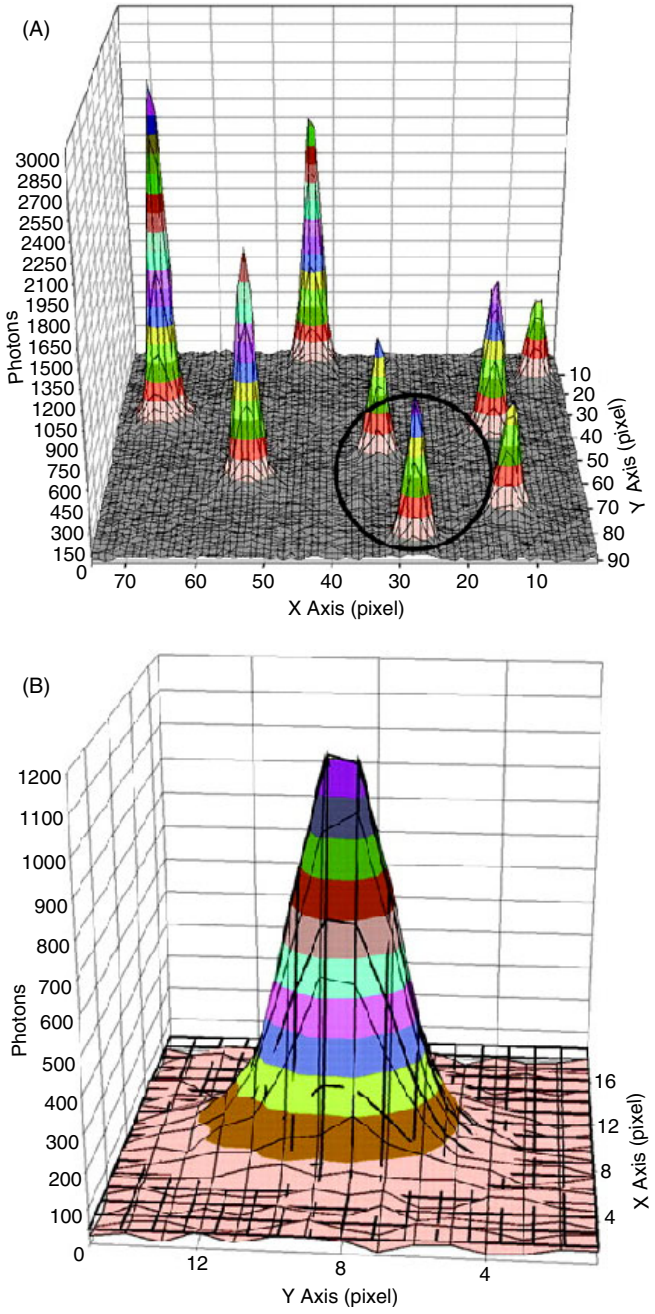

Figure 1. (A) Pixellated images of individual Cy3 dyes immobilized on a glass coverslip. The image was taken by objective-type TIR with 0.5 s integration time. (B) The PSF circled in (A) has a FWHM of 287 nm, and the signal-to-noise ratio of 32. The Gaussian curve fit (solid black line) yielded a precision of 1.3 nm in localization of the centre.

2. Applications to processive molecular motors

2.1. Myosin V

Applications of FIONA to biological systems first started with myosin V. Like most of the processive motors, myosin V is a dimeric protein. The coiled-coil domain, also called the

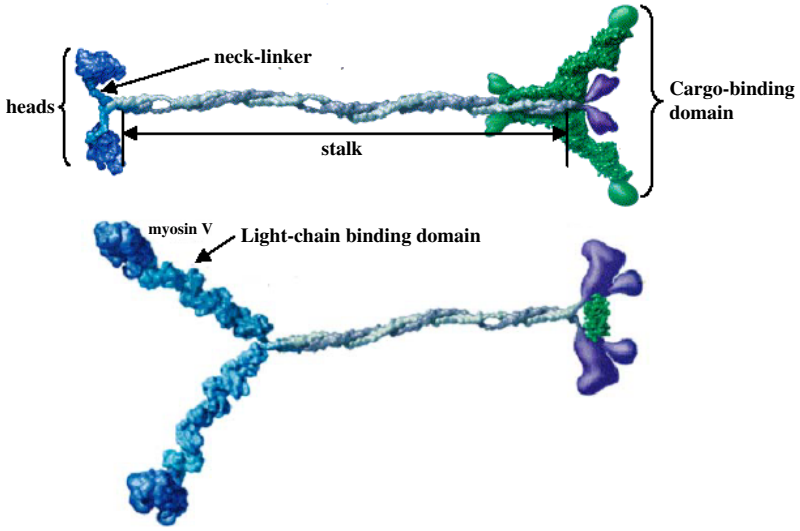

Figure 2. Both kinesin and myosin V are dimeric proteins that walk processively on their tracks. The dark blue regions are the motor domains capable of nucleotide hydrolysis and force production. The coiled-coil region, the stalk, links the head regions to the cargo binding domains. Figure is modified from [14].

stalk, connects the two monomers to each other, and forms the cargo binding domain (figure 2). Each monomer has a 24 nm long light chain binding domain which has six calmodulin binding sites [8, 9]. These long legs enable myosin V to take steps of ∼37 nm per hydrolysed ATP molecule, the longest known step size. Like nearly all myosins (except myosin VI), myosin V moves towards the plus end of actin [10, 11]. The ATP hydrolysis and force generation take place in the actin binding head domain, i.e. the motor domain. Each motor can take hundreds of consecutive steps before myosin V detaches from the actin filament, carrying the cargo for several microns. The cargo of these motors can be pigment granules, membranous organelles, secretary vesicles, or mRNA. Defects in myosin V cause pigmentation and neurological diseases [12–14].

By immobilizing actin filaments on a glass surface, we formed a quasi-1D network on which myosin molecules can walk. This motion can be clearly observed by using TIRF microscopy since we have labelled the protein calmodulin with a single bifunctional rhodamine, and these labelled calmodulins are exchangeable with the calmodulins of myosin V molecules. Two major models were suggested for explaining the stepping mechanism of processive motors: the inchworm model, and the hand-over-hand model (figure 3). According to the inchworm model, one of the heads always leads and both heads move by 37 nm at each step, which results in 37 nm displacement of the stalk. In this model, regardless of where in the structure a dye is placed, one should observe a 37 nm displacement at every step.

The hand-over-hand model proposes quite a different picture in which the trailing and leading heads swap at every step (figure 3). In this model the trailing head is displaced by 74 nm—twice the centre of mass—while the leading head is stationary. Hence, if one of the motors, or heads, is labelled with a dye, the observed displacements for this dye will be 74 and 0 nm sequentially. If the dye is labelled on the leg (i.e. the light chain region), then these values will be $37 + 2x$ and $37 - 2x$, where x is the average distance from the stalk. The FIONA results have shown that the step sizes vary depending on the location of the labelled calmodulin on the myosin light chain domain, and the dye alternates between a long stepping

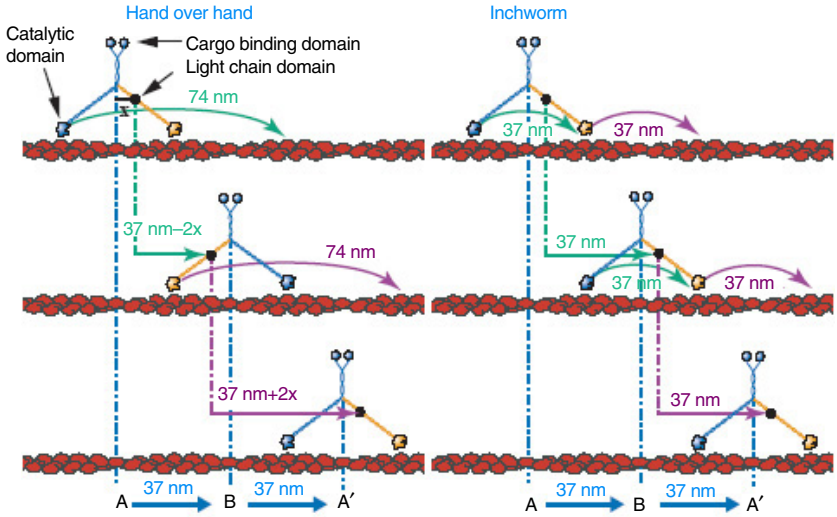

Figure 3. The hand-over-hand model suggests that, in taking a 74 nm step, the rear head passes by the front head while the front head is stationary. Thereby, the heads move 74 and 0 nm steps sequentially. If the marker is on the light chain the FIONA localization will give $37 - 2x$ and $37 + 2x$ for alternating steps, where x is the distance between the marker and the centre of myosin V. In the inchworm model the marker moves a constant 37 nm in each step regardless of its position on the molecule.

motion (e.g. 74 nm) and a short stepping motion (e.g. 0 nm; see figures 4(A) and (B)). This indicates that myosin V walks in a hand-over-hand fashion [7].

2.2. *Conventional kinesin*

Unlike myosin family motors, conventional kinesin (simply kinesin) moves on microtubules. Similar to myosin V, kinesin is also a dimer and has two motor (or head) domains capable of hydrolysing ATP (figure 2). The two heads of kinesin are 8 nm apart, which is the distance between two adjacent tubulin heterodimers on a single protofilament of a microtubule. The motor domains are attached to neck linkers that can undergo conformational changes depending on the nucleotide state of the motor [15]. Neck linkers are connected to the coiled-coil region which leads to the cargo binding domain. The cargo transported by kinesin in a cell varies from membranous organelles to mRNAs. Kinesin mutations can result in neurological diseases in mammals [16].

In our experiments we have immobilized axonemes, microtubule-rich structures which are more stable than single microtubules, on a glass coverslip. One of the head domains of kinesin is labelled with a single Cy3 molecule. The average head displacement calculated by FIONA is found to be 17.3 nm per step. A dwell time histogram also shows that the dye moves alternatingly with 0 and 17.3 nm steps. These findings show that kinesin walks in a hand-over-hand manner [17] (figure 4(C)).

2.3. *Myosin VI*

Myosin VI, similarly to the other members of the myosin family, has three domains in its structure: a head domain (N terminus) which binds to actin and shows ATPase activity, a neck domain, which contains calmodulin binding sites, and a tail domain that binds to

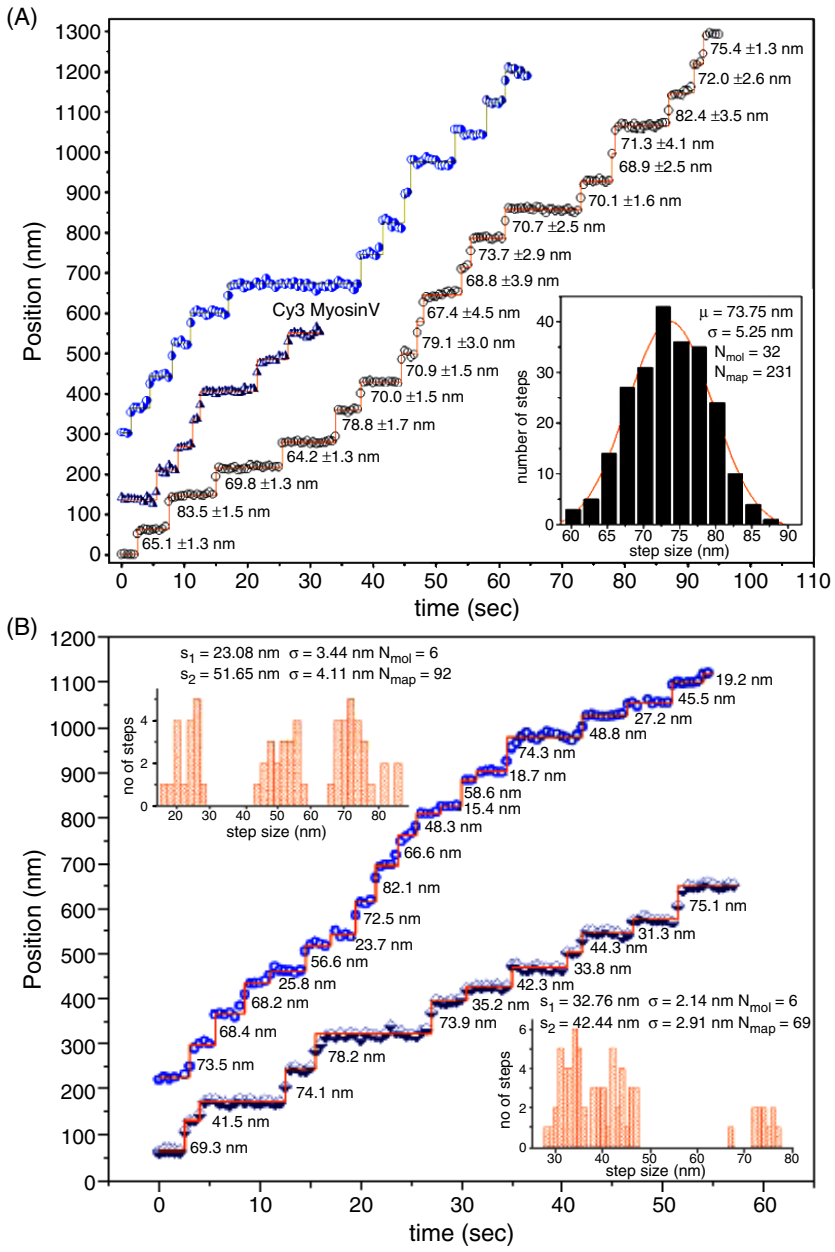

Figure 4. (A) Traces of three different myosin V molecules with an average step size of 74 nm. (B) As the position of the dye changes (different calmodulins are labelled) on the neck linker, step sizes vary giving an indication of the hand-over-hand model. (C) Stepping pattern of an individual head of kinesin. The average step size of 17 nm (double the distance between the head domains) and the kinetic analysis of the dwell time histogram (left inset) which is a convolution of 0 and 16 nm steps strongly suggest that kinesin walks hand-over-hand.

cargo [18]. Uniquely in the myosin family, myosin VI moves towards the negative (pointed) end of actin [19]. It is not certain at the moment whether myosin VI acts as a monomer, a dimer, or possibly both, *in vivo*. Expressed full length myosin VI has been shown to be

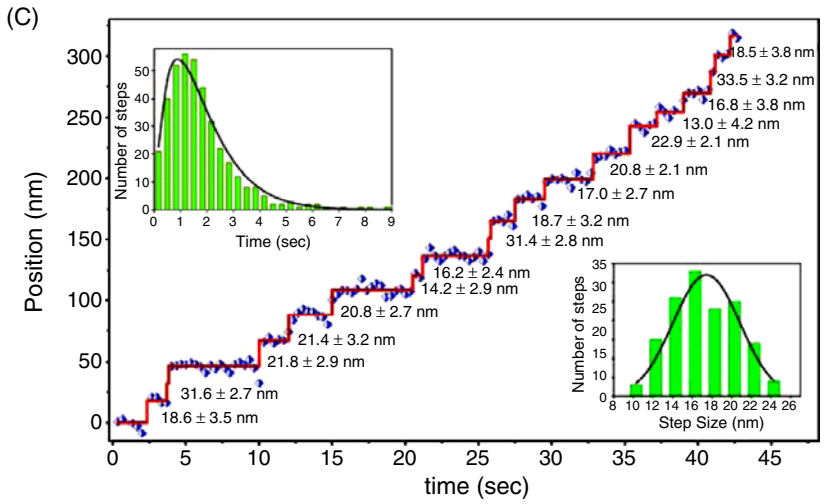

Figure 4. (Continued.)

predominantly a monomer and to be non-processive [20]. However, *in vitro* motility assays showed that dimerized constructs of myosin VI are processive [21, 22]. In addition, optical trap experiments showed that myosin VI acts both as an anchor and as a transporter depending on the applied load [23]. This multifunctionality has been interpreted as evidence for myosin VI acting both as a dimer and as a monomer *in vivo*. The FIONA measurements on myosin VI have been performed on dimerized constructs and have resulted in very intriguing results.

Myosin VI has only two calmodulin binding sites forming the light chain domain [24]. Hence the lever arm is 8–10 nm long. However, both the FIONA measurements [21] and the optical trap measurements [22, 23, 25] have reported a step size of 30 nm. The power stroke due to the lever arm of a monomeric myosin VI (i.e. one head) is measured to be ∼12 nm [26]. Such a large discrepancy in the step size and the lever arm length has challenged the validity of the lever arm mechanism which was successfully applied to both myosin V and kinesin.

In vitro motility assays on kinesin and myosin V have shown that the step size of these motors consists of two parts: a power stroke and a biased diffusive search. For example, myosin V has a 25 nm power stroke, followed by a 12 nm biased diffusive search [11]. The power stroke of these motors has a size comparable to their lever arm length, and the remaining part of the step is due to a biased diffusion which follows the power stroke. The large discrepancy between the step size and the length of the light chain domain in myosin VI required modifications to the presumed structure and the walking mechanism of this motor. Two possible scenarios were considered: there should be a rigid extension to the lever arm, which would result in a larger displacement due to the power stroke, or there should be a flexible region in the structure which would enable a longer diffusive search. Now we will summarize the pioneering FIONA measurements, by Yildiz *et al*, which favoured the flexible extension scenario [21].

Yildiz *et al* used dimerized constructs of myosin VI which were labelled either on the motor domain with eGFP, or on the distal end of the two calmodulins with Cy3. The eGFP labelled molecules showed that each motor moves on average by 55.2 ± 19.6 nm, and similarly the Cy3 labelled molecules showed an average displacement of 63.3 ± 16.7 nm (figure 5). The broad distribution of the step size (3–4 times larger than the distribution in myosin V) was the first observation which favoured a flexible rather than a rigid structure contributing to the

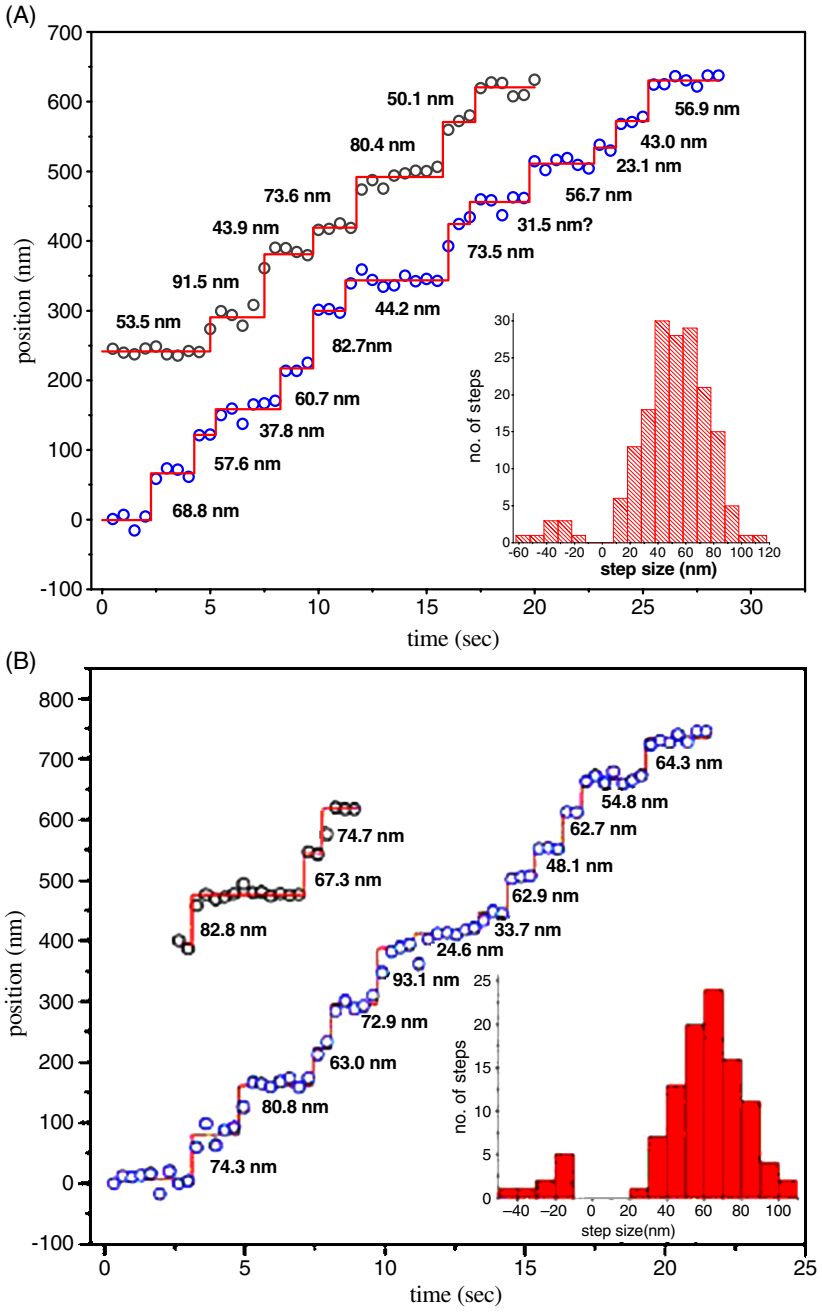

Figure 5. Stepping traces of myosin VI molecules labelled with (A) cy3 and (B) eGFP molecules.

step. Another interesting observation of this study was the large fluctuations, ∼7 nm, observed around the mean position of Cy3 molecules which were attached to the distal calmodulin site. Such large fluctuations were not observed for the eGFP molecules attached to the motor domain of myosin VI, nor for the Cy3 molecules attached to the calmodulin sites of myosin V [7]. This

point was further explored in different nucleotide conditions and different laser powers. The resolution in localizing the Cy3 molecules on the calmodulin binding site increased with increasing laser power as expected from simple theoretical considerations in rigor or the ADP state. However, no enhancement was observed in the resolution as the laser power was increased in the ATP state. This has been considered as evidence for the distal calmodulin site undergoing significant fluctuations, and hence being in the proximity of a flexible region. Finally, Paircoil simulations showed that the first 42 amino acids following the IQ motif have a low probability of forming a coiled coil, and hence could exist as a flexible region in the structure of myosin VI. Recent optical trap experiments have conclusively showed that a flexible region is essential for the large step size of myosin VI [22, 26].

2.4. SHRImP review

FIONA has been successfully applied to various molecular motors labelled with a *single* fluorophore. The low concentration of fluorophores in FIONA enabled localization of the centre point of a single PSF (without any overlap from PSFs of other fluorophores), and hence a 1 nm 'accuracy' was obtained. However, the extension of the technique to 1 nm resolution between multiple fluorophores residing within a diffraction limited spot was still not possible due to overlapping PSFs of different fluorophores. Two techniques were developed as a solution to this problem. The first one is single-molecule high resolution imaging with photobleaching (SHRImP), which was introduced by Gordon *et al* [27]. This technique was independently developed by Qu *et al* [28] and called nanometre-localized multiple single-molecule fluorescence (NALMS). The second technique is called two-colour FIONA [29, 30], or more colourfully, SHREC—single-molecule high resolution colocalization [31].

The PSFs of two closely separated dyes (closer than the diffraction limit) cannot be resolved simultaneously if the dyes have similar excitation and emission spectra. To bypass this limitation, the two-colour FIONA experiments used two dyes of different emission colours. For example, Churchman *et al* used Cy-3 (emission peak at 570 nm) and Cy-5 (emission peak at 670 nm) to label each head of myosin V dimer to study the motility of this motor [31]. Another example of this technique is the study by Warshaw *et al* in which the heads of myosin V were labelled with two quantum dots with emission spectra centred at 565 or 655 nm [30]. This technique is very useful for *dynamically* tracking two closely separated dyes. However, it comes with significant complications which might hinder its establishment as a common technique. First of all, labelling the sample with two different dyes is significantly more difficult than labelling with just one dye. Secondly, the detection optics is more involved since dual-band filters, and in the case of organic dyes [29] two lasers instead of one, are necessary. (Quantum dots can be excited with the same laser [32].)

SHRImP or NALMS on the other hand utilizes the sequential photobleaching of the fluorophores to distinguish between closely separated dyes. In the case of two fluorophores, there are two critical time intervals: the first one is when both fluorophores emit photons, and the second is when one of the fluorophores photobleaches and only one emits photons (figure 6). In the first interval the resulting PSF is the addition of the PSFs from the two dyes, and in the second interval the PSF of only one dye is observed. The subtraction of the PSF of the second interval from the PSF of the first (i.e., the total PSF) results in the PSF of the other dye. In this way, it is possible to determine the position of each dye, and hence the distance between them. Figure 6(B) shows a graphical illustration of how sequential photobleaching can be used to differentiate between two closely spaced dyes.

Gordon *et al* demonstrated this technique by measuring the distance between fluorophores attached to the ends of double-stranded DNA while the DNA was immobilized to the surface

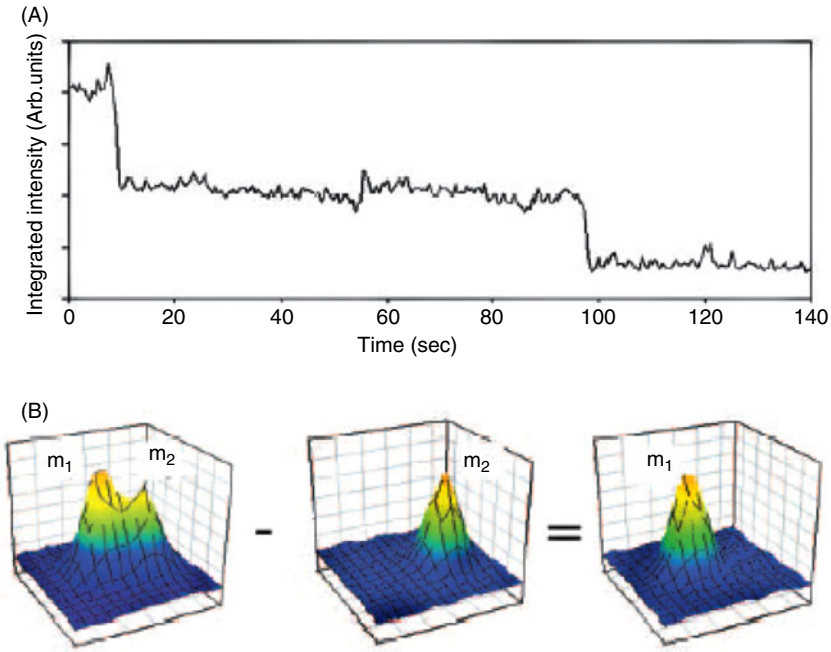

Figure 6. (A) A plot of total integrated intensity versus time for two closely spaced Cy3 molecules, showing a two-step photobleaching behaviour. (B) The PSF of the dye that photobleached first as calculated from the total PSF and PSF of the dye that photobleached second.

and the ends of the DNA were labelled with Cy3 dyes. The lengths of the DNA molecules used in the study were 30, 40, and 51 base pairs long. These lengths are much shorter than the persistence length of the double-stranded DNA (150 base pairs); hence the DNA molecules are immobilized on the surface in a straight and rigid configuration. The corresponding distances between the ends of the DNA were 10.2, 13.6, and 17.3 nm assuming that each DNA base pair is 3.4 Å long. The SHRImP analysis resulted in 10.7 ± 1.0 nm, 13.0 ± 0.5, and 17.7 ± 0.7 nm separations respectively, in excellent agreement with the lengths of the DNA molecules [27].

Shortly after the publication of SHRImP study by Gordon *et al* another study was published in which the same technique was independently developed by Qu *et al* [28]. In this study, the authors used exactly the same methods, with some differences in the computational algorithm for analysing the data, and showed that it is possible to differentiate between three or more fluorophores within a diffraction limited spot. Qu *et al* demonstrated that they can localize individual DNA nucleotides by registering the positions of photobleaching dyes in each frame of image acquisition. A reconstruction of these spots results in a DNA map which, in principle, can be arbitrarily dense. An earlier study by Braslavsky *et al* has also shown that sequence information from a single DNA molecule can be attained by registering photobleaching of non-natural fluorescent bases as they bind to a single-stranded substrate [33].

The first application of SHRImP to a molecular motor was made by Balci *et al* [34]. In this study, the two heads of myosin VI were labelled with eGFP molecules, and the interhead separation, rather than the step size, was measured. This study was motivated by cryo-EM images which showed the heads of a myosin VI dimer bound to adjacent actin monomers [35] (i.e. a few nanometres apart). In the simplest hand-over-hand model, the separation between the heads is expected to be 30 nm regardless of which head took the last step (figure 7(A)).

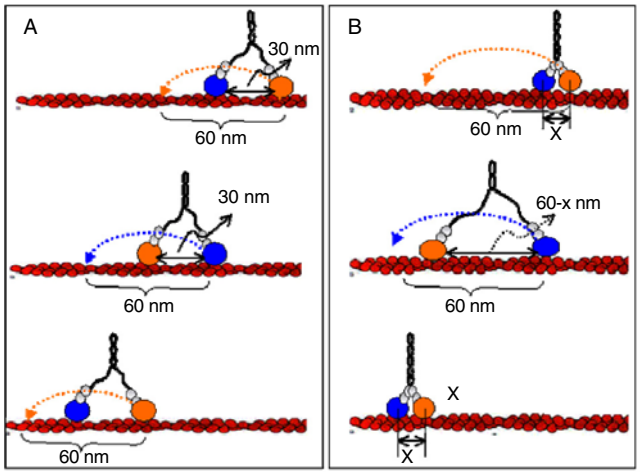

Figure 7. (A) Hand-over-hand mechanism of walking. (B) An alternating model of motility in which the separation between the myosin heads alternates between x and $60 - x$ nm, while each head still takes 60 nm steps sequentially.

However, the cryo-EM images brought up an alternating walking model: the asymmetric hand-over-hand model. In this model, the individual heads still move by 60 nm at each step, but the interhead separation alternates between a small (x, where 5 nm $< x <$ 30 nm) and a large ($60 - x$) distance (figure 7(B)). Such a model would be in complete agreement with the published FIONA, or optical trap, experiments, since the model presumes that the heads alternately take 60 nm steps. In order to distinguish this asymmetric hand-over-hand model from the symmetric one, it is necessary to measure the separation between the two heads, rather than the step size.

According to the symmetric hand-over-hand model, the interhead separations measured for different dimers should be concentrated at 30 nm. On the other hand, in the asymmetric hand-over-hand model the interhead distance should be concentrated at two distinct separations: x and 60 nm. Balci *et al* showed that the interhead separation histogram shows a single peak at 29.2 ± 0.8 nm, as determined from a Gaussian fit of the form $y = y_0 + a \exp[-0.5([x - x(0)]/b)^2]$ to the interhead separations histogram, in excellent agreement with the symmetric hand-over-hand model (see figure 8) [34]. However, due to the broadness of this peak, the authors were not able to rule out the possibility of two closely separated peaks. In order to set a limit for the resolution of the data in differentiating between the two possibilities, the data were fitted with functions which contain two Gaussians, i.e. $y = y_0 + a \exp[-0.5([x - x_1(0)]/b)^2] + c \exp[-0.5([x - x_2(0)]/d)^2]$, with different constraints on the fitting parameters. (Two such fits are shown in figure 8.) This analysis resulted in 14 nm as the upper limit of the asymmetry; i.e. the interhead separations cannot be more asymmetric than $x = 23$ nm and $60 - x = 37$ nm.

2.5. Pushing the limits up

The *in vitro* studies on molecular motors have resulted in very powerful techniques, such as FIONA, which enabled the study of these biological systems with nanometre spatial and sub-second temporal resolution. However, ultimately a complete understanding of the functions and working principles of these systems is possible only if they can be studied within their

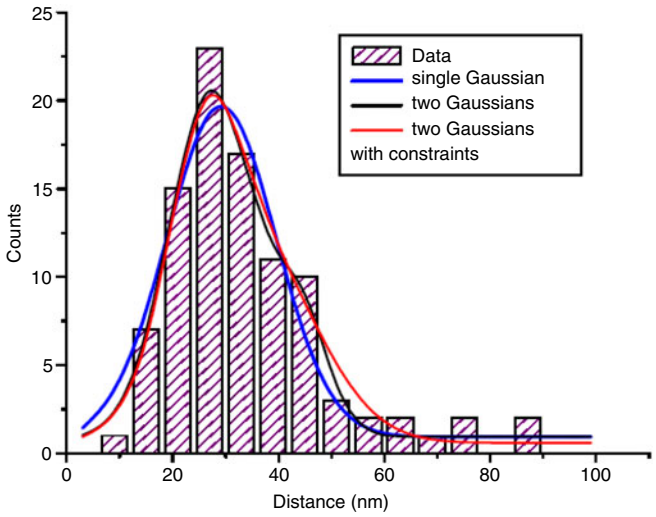

Figure 8. Histogram of measured separations between the myosin VI heads and three Gaussian fits to the data. The blue curve is a single Gaussian fit representing the hand-over-hand model, the black curve is an unconstrained fit of two Gaussians, and the red curve is a fit of two Gaussians with constraints.

natural environment, i.e. *in vivo*. At this point the challenging question is 'Is FIONA possible *in vivo*?'

Before answering such a question, the complexities of an *in vivo* motility experiment should be considered. First of all, the high background fluorescence of a cell makes it crucial to use a relatively bright marker. Moreover, at physiological ATP concentrations, the molecular motors move at much higher stepping rates than those typical for *in vitro* studies. This requires a faster image acquisition system to resolve the stepwise motion. Fast image acquisition reduces the photon integration time, and hence nanometre resolution becomes more difficult to achieve since fewer photons are collected. One other difficulty arises in labelling specificity: in a live cell there are a vast variety of molecular motors and other biological species. Hence, being able to determine which motor is responsible for the motility is a non-trivial task.

Taking into account all these obstacles we have decided to work on Drosophila (fruit fly) S2 cells that express the protein GFP-skl constitutively. GFP-skl is a green fluorescent protein that has a signalling peptide tail (skl) which ensures that all the GFPs produced are taken to the peroxisomes in the S2 cells. In other words, the peroxisomes are labelled with thousands of GFP molecules. Another advantage of working with S2 cells is that when they are cultured on concavalin A treated coverslips, and treated with drugs capable of breaking down actin filaments (such as latrunculin B or cytochalasin D), they grow processes filled with bundles of microtubules (figure 9(A)). The peroxisomes carried in these processes move in a highly linear fashion. Moreover, by eliminating the filamentous actin, we ensure that the peroxisome movement is due to microtubule dependent motors since actin dependent motors cannot operate.

Eliminating the actin dependent molecular motors is an essential ingredient in simplifying the studying of *in vivo* motility since the problem is then reduced to just studying microtubule dependent molecular motors. However, there are still quite a number of motors (such as conventional kinesin, kinesin 2, NCD, and dynein) remaining as possible organelle transport *in vivo* candidates. To eliminate these possibilities, we have used double-stranded RNA

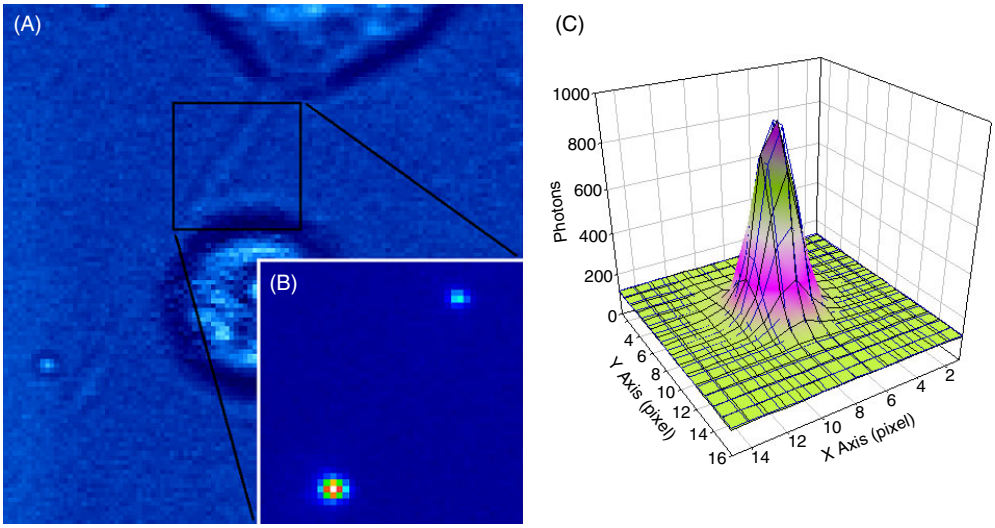

Figure 9. (A) S2 cell growing a thin process upon loss of actin filaments. (B) Fluorescence image of two peroxisomes in the process. (C) The emission pattern of the GFP labelled peroxisome can be well fitted with a 2D Gaussian and the peak can be determined with 1.4 nm accuracy and 1.1 ms integration time.

interference (RNAi) in order to determine which motors are actively involved in the peroxisome movement. Using RNAi is a very powerful technique for 'knocking down', i.e. eliminating, proteins or different kinds of motors in a cell. Consequently, by using RNAi and monitoring whether the motility is affected, the type of motors involved in transport can be determined. When double-stranded RNA homologous to the mRNA of a specific gene is introduced in a cell, it initiates a process that destroys all the mRNA of that specific gene produced, and hence prevents the expression of that gene. In S2 cells, RNAi works very efficiently, so up to 90% of proteins can be eliminated [36]. RNAi experiments done on microtubule dependent motors have shown that peroxisome transport in S2 cells is severely reduced in the absence of either cytoplasmic dynein or conventional kinesin (simply kinesin), whereas using RNAi for the other kinesin family proteins failed to inhibit peroxisome motility. These results indicate that dynein and conventional kinesin are responsible for the peroxisome movement.

As we have mentioned before, kinesin carries its cargo to the (+) end of a microtubule, i.e. away from the nucleus. Kinesin's counterpart, dynein, works in the opposite direction, and it carries the cargo to the (−) end. This makes the directionality of the motion a crucial element in determining which one of the two motors is active at a given instant. In a cell, the microtubules are aligned in such a way that their (−) ends are located at the centre while their (+) ends extend to the periphery of the cell. When studying microtubule dependent transport in processes, the diameter of the process is the important parameter to be careful about (processes are preferred for this study due to the highly linear motion of peroxisomes in them). In thick processes, microtubules can wrap around, making their (+) and (−) ends point in arbitrary directions. On the other hand, for in thin processes (diameter smaller than $\sim$1 μm), we showed that over 90% of microtubules are oriented properly. Consequently, we chose to analyse only these processes: we did not include in our analysis the peroxisomes found in thick processes.

So far we have proven that GFP labelled peroxisomes of S2 cells can be used as excellent markers for studying how kinesins and dyneins work as organelle transporters *in vivo*. Now the question we have to answer is: 'Can we use FIONA on GFP labelled peroxisomes?'

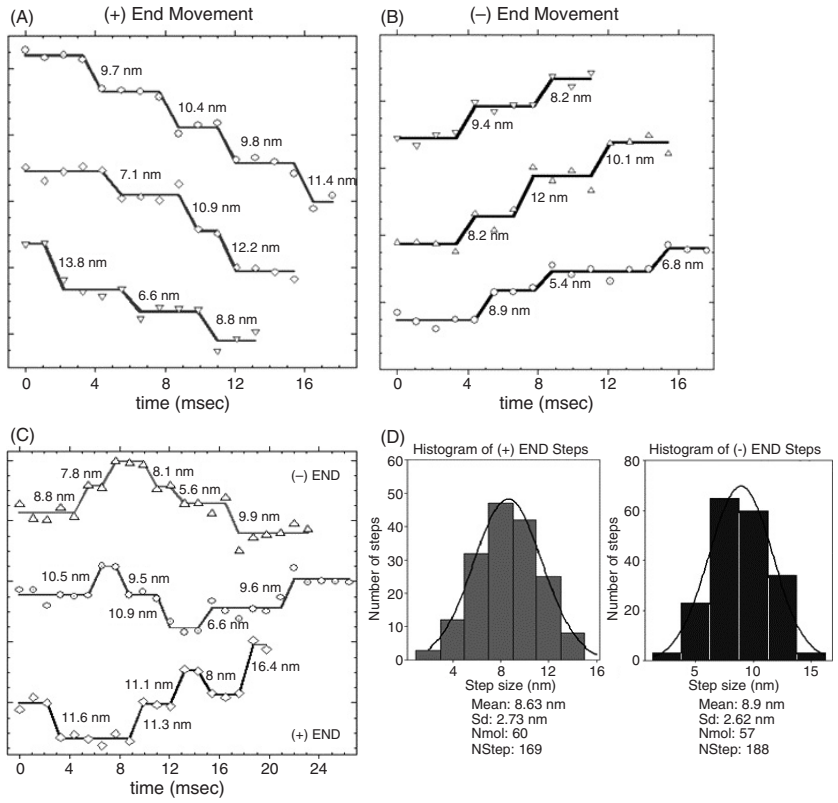

Figure 10. The stepwise displacement of peroxisomes driven by kinesin (A) and dynein (B) motors. (C) Switching between the (+) and (−) end directed movements in a stepwise manner. (D) Step size histograms of kinesin and dynein motors.

Fortunately, the answer is yes. The peroxisomes can be localized to within 1.4 nm accuracy at 1.1 ms integration time (figure 9(C)). This is about 500 times faster than previously reported FIONA results for *in vitro* motility experiments. This high spatial and temporal resolution enabled us to see the transport of peroxisomes in a step-by-step manner in both anterograde (plus end directed) and retrograde (minus end directed) motions (figures 10(A)–(C)). In perfect agreement with the previous *in vitro* assays, we have observed that the average step sizes of kinesin and dynein are both about 8 nm [37, 38].

For years the most challenging question concerning the intracellular organelle transport has been: 'What is the mechanism that switches the direction of transport?' Two major models are a tug-of-war, or a coordination, of opposite polarity motors [39]. The tug-of-war model suggests that motors of both polarities (kinesin and dynein) exert force on the same cargo simultaneously, with the result that the net displacement (direction) of the cargo is determined by the stronger side. In other words, if the number of motors times the force of each motor pulling the cargo in a particular direction is more or less than that of the opposite direction, then the side producing more force is going to be dominant. According to this model there is going to be an enduring strain on the linkers of the carrier proteins that link the cargo to the motor domain. On the other hand, according to the coordination model, the motors of opposite polarity do not work on the same cargo at the same time. Rather, they are controlled by a mechanism which can turn off motors of a particular direction while turning on the other

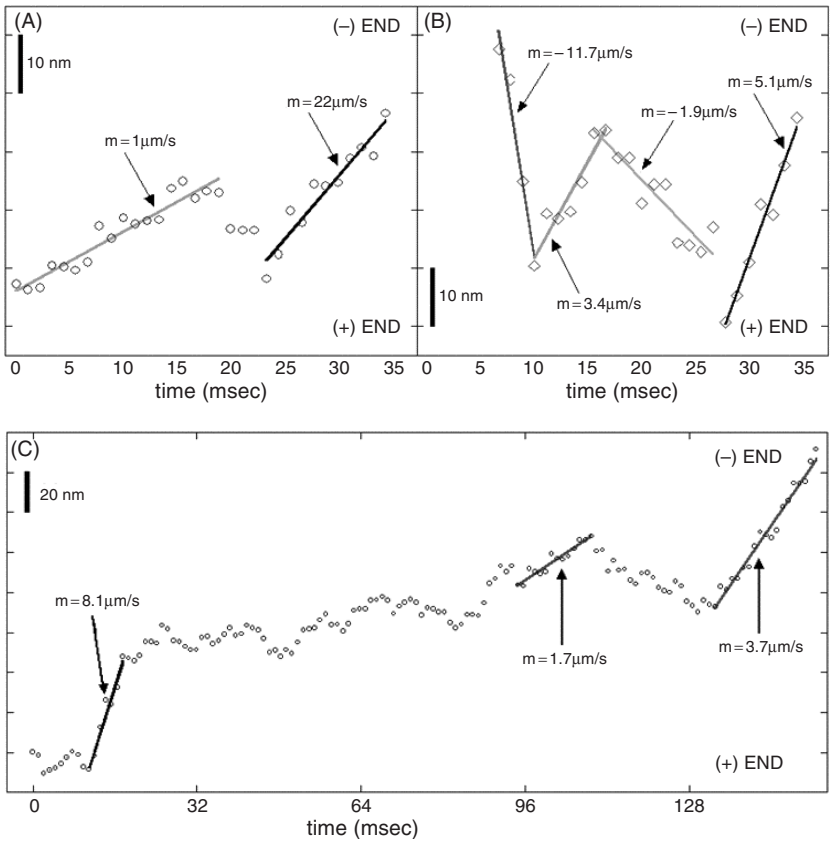

Figure 11. (A)–(C) Peroxisome transport occurring at various speeds. Peroxisomes can be transported as fast as 11.7 μm s^{-1}.

polarity motors. This fast switching may be done by a small molecule that can turn on and off kinesin and dynein alternatingly in a very short timescale (less than a millisecond). Another possible scenario (which is also considered a coordination) is that where kinesin and dynein pull against one another until one of them detaches from the cargo or the microtubule and the other motor independently carries the cargo. On the basis of these definitions, our results favour the coordination model: if the opposite polarity motors were in a tug-of-war, any 8 nm step taken by the motors would move the cargo less than 8 nm when opposite polarity motors are simultaneously active on the same cargo (due to the compliance of the linker regions). We have not seen such a degradation in the step sizes in either anterograde or retrograde motions. Rather the average step size was 8 nm for both kinesin and dynein (figure 10(D)), in agreement with the previous *in vitro* results.

One other striking finding was the various organelle transport rates in S2 cells. The highest speed a microtubular motor protein can reach *in vitro* is found to be of the order of 1 μm s^{-1} [40–42]. In contrast, we observed that peroxisomes can be transported at various speeds (figures 11(A)–(C)), sometimes as fast as 12 μm s^{-1}. When a histogram of the speed of runs longer than 15 nm is made, we see that the results are spiked and the peaks are evenly distributed in (+) and (−) end directed motions (figures 12(A) and (B)). This suggests that each peak corresponds to a different number of motors carrying the cargo at every instant.

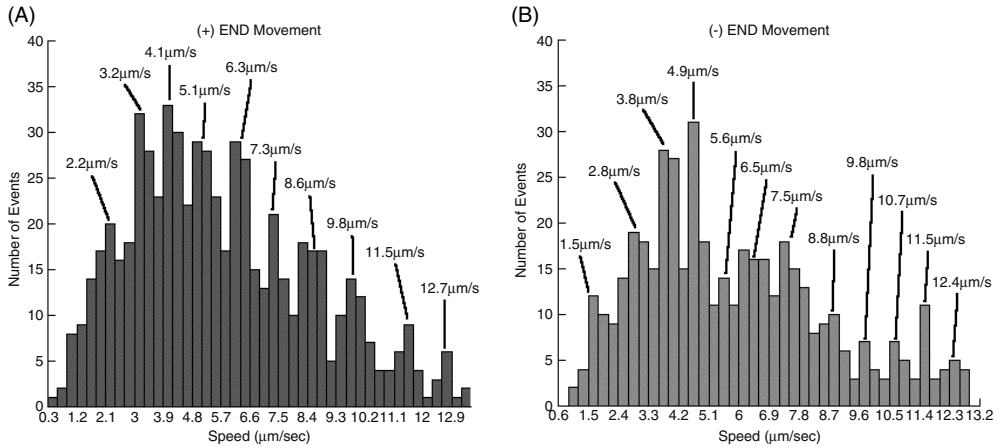

Figure 12. Histogram of speeds of runs (only runs longer than 15 nm are considered) in both plus (A) and minus (B) end directed movements. Both histograms are spiked and the peaks are evenly distributed, suggesting that they correspond to different numbers of motors.

For kinesin, a motor with a very high duty ratio, how this cooperation is achieved is another question which does not have a clear answer yet.

In conclusion, single-molecule biophysics and single-particle tracking techniques have proven to be invaluable tools for studying biological phenomena at the microscopic level. In particular, FIONA and its extensions to multicolour and multifluorophore realms have made significant contributions to the study of molecular motors, and are now mature enough to be applied to other fields of single-molecule biophysics.

Acknowledgments

We thank the National Institutes of Health for their support through grants AR44420 and GM068625.

References

[1] Hecht E 2002 *Optics* (San Francisco, CA: Addison-Wesley)
[2] Bevington P R and Robinson D K 2002 *Data Reduction and Error Analysis for the Physical Sciences* (New York: McGraw-Hill)
[3] Cheezum M K, Walker W F and Guilford W H 2001 *Biophys. J.* **81** 2378
[4] Thompson R E, Larson D R and Webb W W 2002 *Biophys. J.* **82** 2775
[5] Kural C, Kim H, Syed S, Goshima G, Gelfand V I and Selvin P R 2005 *Science* **308** 1469
[6] Axelrod D 1989 *Methods Cell Biol.* **30** 245
[7] Yildiz A, Forkey J N, McKinney S A, Ha T, Goldman Y E and Selvin P R 2003 *Science* **300** 2061
[8] Espindola F S, Suter D M, Partata L B, Cao T, Wolenski J S, Cheney R E, King S M and Mooseker M S 2000 *Cell Motil. Cytoskeleton* **47** 269
[9] Cheney R E, O'Shea M K, Heuser J E, Coelho M V, Wolenski J S, Espreafico E M, Forscher P, Larson R E and Mooseker M S 1993 *Cell* **75** 13
[10] Mehta A D, Rock R S, Rief M, Spudich J A, Mooseker M S and Cheney R E 1999 *Nature* **400** 590
[11] Veigel C, Wang F, Bartoo M L, Sellers J R and Molloy J E 2002 *Nat. Cell Biol.* **4** 59
[12] Reck-Peterson S L, Provance D W Jr, Mooseker M S and Mercer J A 2000 *Biochim. Biophys. Acta* **1496** 36
[13] Vale R D 2003 *J. Cell Biol.* **163** 445
[14] Vale R D 2003 *Cell* **112** 467

[15] Rice S *et al* 1999 *Nature* **402** 778
[16] Reid E *et al* 2002 *Am. J. Hum. Genet.* **71** 1189
[17] Yildiz A, Tomishige M, Vale R D and Selvin P R 2004 *Science* **303** 676
[18] Berg J S, Powell B C and Cheney R E 2001 *Mol. Biol. Cell* **12** 780
[19] Wells A L, Lin A W, Chen L Q, Safer D, Cain S M, Hasson T, Carragher B O, Milligan R A and Sweeney H L 1999 *Nature* **401** 505
[20] Lister I, Schmitz S, Walker M, Trinick J, Buss F, Veigel C and Kendrick-Jones J 2004 *Embo J.* **23** 1729
[21] Yildiz A, Park H, Safer D, Yang Z, Chen L Q, Selvin P R and Sweeney H L 2004 *J. Biol. Chem.* **279** 37223
[22] Rock R S, Rice S E, Wells A L, Purcell T J, Spudich J A and Sweeney H L 2001 *Proc. Natl Acad. Sci. USA* **98** 13655
[23] Altman D, Sweeney H L and Spudich J A 2004 *Cell* **116** 737
[24] Bahloul A *et al* 2004 *Proc. Natl Acad. Sci. USA* **101** 4787
[25] Okten Z, Churchman L S, Rock R S and Spudich J A 2004 *Nat. Struct. Mol. Biol.* **11** 884
[26] Rock R S, Ramamurthy B, Dunn A R, Beccafico S, Rami B R, Morris C, Spink B J, Franzini-Armstrong C, Spudich J A and Sweeney H L 2005 *Mol. Cell* **17** 603
[27] Gordon M P, Ha T and Selvin P R 2004 *Proc. Natl Acad. Sci. USA* **101** 6462
[28] Qu X, Wu D, Mets L and Scherer N F 2004 *Proc. Natl Acad. Sci. USA* **101** 0402155101
[29] Yildiz A, Goldman Y E and Selvin R P 2005 Two-color FIONA, in preparation
[30] Warshaw D M, Kennedy G, Work S, Krementsova E, Beck S and Trybus K 2005 *Biophys. J.* **88** L30
[31] Churchman L S, Okten Z, Rock R S, Dawson J F and Spudich J A 2005 *Proc. Natl Acad. Sci. USA* **102** 1419
[32] Michalet X, Pinaud F F, Bentolila L A, Tsay J M, Doose S, Li J J, Sundaresan G, Wu A M, Gambhir S S and Weiss S 2005 *Science* **307** 538
[33] Braslavsky I, Hebert B, Kartalov E and Quake S R 2003 *Proc. Natl Acad. Sci. USA* **100** 3960
[34] Balci H, Ha T, Sweeney H L and Selvin P R 2005 *Biophys. J.* **89** 413
[35] Nishikawa S *et al* 2002 *Biochem. Biophys. Res. Commun.* **290** 311
[36] Rogers S L, Rogers G C, Sharp D J and Vale R D 2002 *J. Cell Biol.* **158** 873
[37] Svoboda K, Schmidt C F, Schnapp B J and Block S M 1993 *Nature* **365** 721
[38] Mallik R, Carter B C, Lex S A, King S J and Gross S P 2004 *Nature* **427** 649
[39] Mallik R and Gross S P 2004 *Curr. Biol.* **14** R971
[40] King S J and Schroer T A 2000 *Nat. Cell Biol.* **2** 20
[41] Nishiura M, Kon T, Shiroguchi K, Ohkura R, Shima T, Toyoshima Y Y and Sutoh K 2004 *J. Biol. Chem.* **279** 22799
[42] Kon T, Nishiura M, Ohkura R, Toyoshima Y Y and Sutoh K 2004 *Biochemistry* **43** 11266